Kalpa Publications in Computing

Volume 22, 2025, Pages 316–329

Proceedings of The Sixth International Conference on Civil and Building Engineering Informatics

Automatic Detection of Building Equipment using Laser Intensity of MLS Point Cloud

Arisa Kobayashi[1] and Tomohiro Mizoguchi[2]

[1] Nihon University, Fukushima, Japan

[2] Sanyo-Onoda City University, Yamaguchi, Japan

mizoguchi@rs.socu.ac.jp

Abstract

Building Information Modeling (BIM) is being increasingly used in the maintenance of buildings. Since 3D models do not exist for old buildings, it is common to create BIM from 3D scanned point clouds. To date, it has become possible to construct simple BIM consisting of major components such as floors, walls, ceilings, and columns almost automatically. However, automatic construction of detailed BIM including building equipment (lighting, air conditioning, fire alarm, etc.) necessary for building maintenance has not yet been achieved. These are often attached to ceilings and walls, and are difficult to recognize because of their small surface area and thickness. In this paper, we propose a method to detect building facilities using laser reflection intensity to automatically construct detailed BIM from point clouds of building by mobile laser scanners (MLS). In this method, first, the effects of distance and incident angle included in the reflection intensity are eliminated based on polynomial approximation, and the reflection intensity value of ceilings and walls composed of the same material is approached to a constant value. Next, since the corrected intensity follows a normal distribution, a set of points that deviate from the normal distribution is extracted as building equipment candidates by thresholding process. Finally, the point cloud is converted into an image representation, and each equipment is extracted using morphological and labeling process. Through various experiments targeting the ceilings and a wall of buildings, the proposed method achieved a high detection rate.

1 Introduction

Building Information Modeling (BIM), which combines 3D shape and attribute information, is being used in the maintenance of buildings. Since 3D models do not exist for old buildings, it is common to create BIM from 3D scanned point cloud. To date, it has become possible to construct simple BIM consisting of major components such as floors, walls, ceilings, and columns almost automatically (Gourguechon et al., 2022). However, it has not yet been possible to automatically

I. Hkust, J. Cheng and Y. Yantao (eds.), ICCBEI 2025 (Kalpa Publications in Computing, vol. 22), pp. 316–329

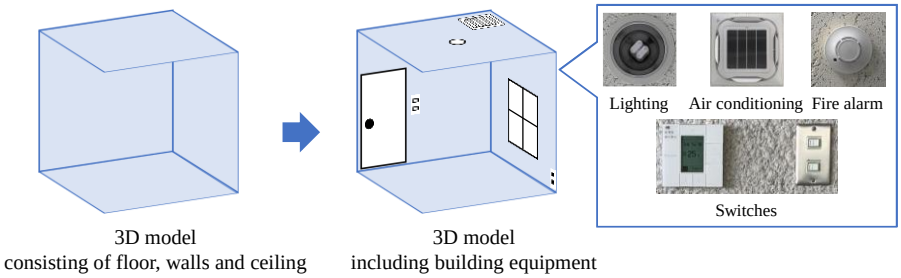

Figure 1. Construction of detailed BIM from point cloud

construct detailed BIM including building equipment (lighting, air conditioning, fire alarms, etc.) necessary for the maintenance of buildings, as shown in Figure 1. These are often attached to the ceiling or wall, and have a small surface area and thickness, making it difficult to recognize them by evaluating only their shape (Hossain et al., 2021). Therefore, a method is needed to detect building equipment from information other than the shape (coordinate values) of the point cloud and incorporate it into simple BIM to construct detailed BIM.

In this paper, we propose a method to detect building equipment using laser reflection intensity contained in the scanned point cloud obtained by a mobile laser scanner (MLS) to automatically reconstruct detailed BIM. Compared to conventional terrestrial laser scanners (TLS), MLS has the advantage of being able to scan a wide area efficiently and has rapidly become popular in recent years (Stefano et al., 2021). Laser reflection intensity is a value that indicates the intensity of reflected light from the target surface. Since it varies depending on the color and material of the target, it is considered to be extremely effective for detecting building equipment in the point cloud. However, since the reflection intensity value obtained from the scanner includes the effects of the scanning distance and incident angle, it is necessary to appropriately exclude them and correct it to a value that reflects only the difference in color and material. Generally, ceilings and walls are wide and flat, and made of the same material, and building equipment of different colors and materials are attached there. Therefore, the basic idea of this study is that if the reflection intensity value of ceilings and walls can be appropriately corrected and approached close to a constant value, point sets with values different from them can be detected as building equipment.

Object recognition in point clouds generally consists of an extraction step, in which partial point clouds corresponding to each object are individually extracted, and a classification step, in which the class of each object (lighting, fire alarm, etc.) is estimated. Of these two steps, this study only deals with the first step, the extraction step. If extraction is possible, we believe that by using the corresponding partial images for each object in the classification step, highly accurate classification will be possible using AI with appropriate image processing.

2 Related Works

2.1 BIM Reconstruction from Point Cloud

There have been several studies on detecting building equipment from point clouds. Akiyama et al. (Akiyama et al., 2023) proposed a method to detect building equipment on the ceiling surface from TLS scanning point clouds. First, as preprocessing, 2D ceiling regions are extracted from the point cloud data and structured. Then, it detects partial point clouds corresponding to each building equipment such as lighting and air conditioning, and then fits circles and rectangles to their boundary points. However, it is difficult to detect objects with small thickness using only the shape information

of the point cloud. In addition, the detection rate decreases when the scanning distance exceeds 5 meters, so the number of scans increases as the target area becomes wider. Note that classification processing was not performed in this study. Pan et al. (Pan et al., 2022) proposed a method to detect building equipment using both images and point clouds. First, two 3D point clouds are obtained by SfM-MVS and laser scanning, and then these are synthesized. On the other hand, it used a convolutional neural network (CNN) on video data to detect and classify building equipment inside a building and added them to the point cloud to construct a detailed BIM. However, since a 3D model is constructed by combining two types of point cloud data, there are problems such as cumbersome processing and a large amount of time. In addition, while object detection using CNN is easy to detect objects with small shape variations such as fire extinguishers and fire alarms, a large amount of training data must be prepared for objects with large shape variations such as ceiling lights. Anjanappa et al. (Anjanappa et al., 2023) also detected and classified building equipment inside a building using CNN on 3D point clouds. However, similar to the above, it is necessary to prepare sufficient training point cloud data to detect a wide variety of building equipment.

2.2 Laser Intensity Correction

The reflectance intensity values obtained from a laser scanner are generally affected by the reflectance of the object as well as the distance, incident angle, sensor characteristics, and atmospheric conditions, so it is not recommended to use them directly without correction (Bai et al., 2023).

When using one scanner to scan in a short time under the same environment, there is no need to consider the effects of the sensor characteristics and atmospheric conditions mentioned above, and the value changes according to the radar equation due to the reflectance of the target, the incident angle, and the distance. Furthermore, these three factors are independent of each other and can be expressed by Equation (1) (Tan & Cheng, 2020).

$$I(\rho,\theta,d) = f_1(\rho)\cdot f_2(\theta)\cdot f_3(d) \tag{1}$$

Where $I(\rho,\theta,d)$ is the initial reflection intensity, f_1, f_2, and f_3 are the functions of reflectance of the target ρ, incident angle θ, and distance d respectively.

Theoretically, the reflection intensity is directly proportional to the cosine of the incident angle and inversely proportional to the square of the distance. However, considering the complexity of the effects of the distance and incident angle, a method of eliminating the effects of the distance and incident angle using a polynomial, as shown in Equation (2), has been found to be effective (Tan & Cheng, 2020).

$$I_{cor}(\rho) = I(\rho,\theta,d)\cdot\frac{\sum_{i=0}^{N_2}\left(\alpha_i {\theta_s}^i\right)}{\sum_{i=0}^{N_2}(\alpha_i\theta^i)}\cdot\frac{\sum_{i=0}^{N_3}\left(\beta_i {d_s}^i\right)}{\sum_{i=0}^{N_3}(\beta_i d^i)} \tag{2}$$

Where α_i and β_i are polynomial parameters, and N_2 and N_3 are the degrees of the polynomial. To estimate the polynomial parameters, it is necessary to derive the relationship between the reflected intensity and the distance or incident angle, and define a correction equation.

One method for calculating the correction equation is to use a target and find the relationship between reflection intensity, distance, and incident angle, respectively. In the method by (Tan & Cheng, 2015), the TLS point cloud was mainly used, and the target was scanned multiple times from different distances and angles in a laboratory, and a polynomial for correction was calculated based on the obtained reflection intensity values. First, the target was scanned from a fixed distance between 0deg and 90deg at small intervals (for example, 5deg pitch) to obtain samples of angle and reflection

intensity. Similarly, it is scanned while changing the distance at a fixed pitch while keeping the angle constant, and it obtains samples of distance and reflection intensity. Least-squares fitting of polynomial to this set of sample points, we can obtain correction equations that express the relationship between the incident angle-reflection and the distance-reflection intensity. However, the correction equation for the distance-reflection intensity is more complicated than that for angle and requires scans at fine intervals up to distances of several tens of meters, which results in problems such as a huge amount of time required for the experiment. Therefore, a method has been proposed to calculate the correction equation for the distance and reflection intensity from the actual scanning point cloud (Tan & Cheng, 2020). First, angle correction is performed as shown in Equation (3) from the correction equation that expresses the relationship between the incident angle and reflection intensity calculated using the target as described above.

$$I_\theta(\rho, d) = I(\rho, \theta, d) \cdot \frac{\sum_{i=0}^{N_2}\left(\alpha_i {\theta_s}^i\right)}{\sum_{i=0}^{N_2}(\alpha_i \theta^i)} \tag{3}$$

The obtained incident angle corrected reflection intensity $I_\theta(\rho,d)$ is a reflection intensity that is affected only by the distance, so the distance-reflection intensity correction equation is calculated using least squares regression on the reflection intensity after incident angle correction. The final corrected reflection intensity $I_{cor}(\rho)$ can be calculated using Equation (2) based on the calculated polynomial parameters.

On the other hand, in addition to the method using the polynomial mentioned above, there is also a method of correction using a look-up table (LUT) (Jeong & Kim, 2018). This method focuses on the fact that the ratio of the reflection intensity of two scanning surfaces at the same distance and incident angle must be the same as the ratio of the reflectance. A LUT is composed of 2D cells with the vertical axis as the distance and the horizontal axis as the incident angle and is created by calculating the average value and standard deviation of the reflection intensity for the distance and incident angle corresponding to each cell. To obtain the data used for creation, a point cloud scanned on a wide plane made of the same material, such as a large wall several meters square, is used as a reference surface. Using this LUT, the reflectance of the reflection intensity of the scanning surface can be estimated as shown in Equation (4).

$$I_{cor}(\rho) \propto I\left(\rho_{ref}\right) \cdot \frac{I(\rho, \theta, d)}{I(\rho_s, \theta, d)} \tag{4}$$

Where the reflection intensity $I(\rho_s,\theta,d)$ of the reference surface is the average value of the reflection intensity corresponding to each cell of the LUT. Also, the true reflectance of the reference surface $I(\rho_{ref})$ is unknown, so it is set arbitrarily.

Different from the above-mentioned method, a method has been proposed to calculate the correction equation using only the obtained scanning point cloud without preparing a correction equation or LUT in advance. For example, when measuring a road surface using a vehicle-mounted LiDAR, if the height between the scanner and the road surface is constant, the incidence angle can be described as a function of the distance. Therefore, as shown in Equation (5), by correcting only the effect of the distance, the incidence angle can also be corrected at the same time (Wan et al., 2019).

$$I_{cor}(\rho) = I(\rho, \theta, d) \cdot \frac{\sum_{i=0}^{N_3}\left(\beta_i {d_s}^i\right)}{\sum_{i=0}^{N_3}(\beta_i d^i)} \tag{5}$$

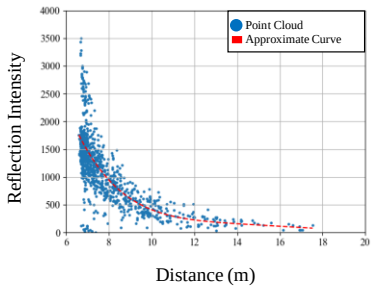

(a) Scatter plots and approximate curves of distance-reflection intensity

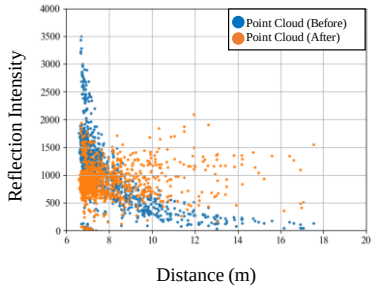

(b) Scatter plots of distance-reflection intensity before and after correction

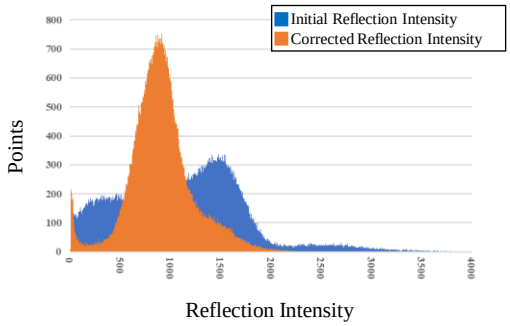

(c) Reflection intensity histogram before and after correction

Figure 2. Reflection intensity correction

The authors have demonstrated a certain degree of effectiveness of the proposed reflection intensity correction through experiments on extracting road markings from MLS point clouds. Although this method requires certain measurement conditions, correction is possible using only the point cloud, and it can be widely deployed in a variety of applications.

3 Method

3.1 Overview of The Proposed Method

In this method, first, the area to be modeled is manually extracted, and preprocessing is performed to sample the point cloud so that the point density is spatially uniform. After that, the effects of distance and incident angle contained in the reflection intensity are eliminated based on polynomial approximation, and the reflection intensity value of walls and ceilings made of the same material is corrected to approach a constant value. Next, since the corrected reflection intensity follows a normal distribution, a set of points that deviate from the normal distribution are extracted as equipment candidates by thresholding process. Finally, the point cloud is converted into a binary image, and each equipment is extracted using morphological and labeling process. In this report, we focus on the area scanned while keeping the distance between the scanner and the scanning surface constant. The details are described below.

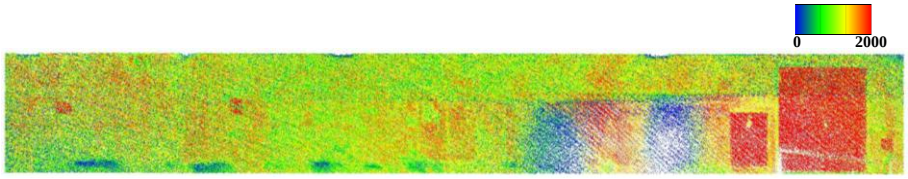

(a) Before correction

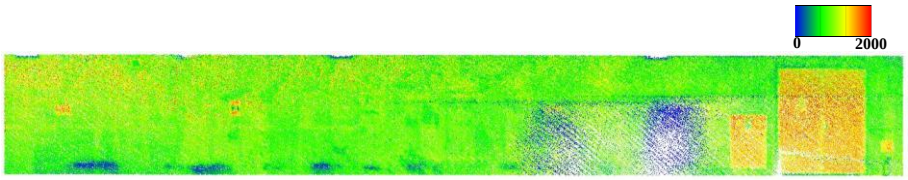

(b) After correction

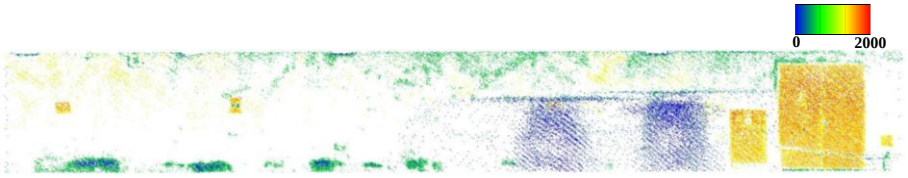

(c) Extracted equipment candidate point cloud

Figure 3. Results of reflection intensity correction on point cloud

3.2 Pre-processing

The point cloud obtained from the scanner is high-density data that includes the surrounding area of the target. Furthermore, as the scanning target becomes wider, the amount of data becomes enormous, ranging from tens of millions to hundreds of millions of points. Therefore, to make the point cloud easier to handle, we use the free point cloud processing software Cloud Compare to cut out the target area and thin out the point cloud at 1 cm intervals.

3.3 Reflection Intensity Correction

In this method, the distance and incident angle are simultaneously corrected using the method of Wan et al. (Wan et al., 2019) introduced in Section 2.2. This method is easier to compensate for than other methods and is considered effective for BIM construction. A scatter plot is created from the scanning point cloud, with the horizontal axis as the distance and the vertical axis as the reflection intensity, and an approximate polynomial is obtained for this set of points by the least-squares method. Referring to the method of Wan et al., the degree of the polynomial was set to $N_3 = 3$. Furthermore, *ds* in Equation (5) was set to the average value of the distance. Figure 2(a) shows the result of superimposing the scatter plot of distance-reflection intensity and the calculated correction equation. Figure 2(b) shows the sample points before and after correction. It can be confirmed that the reflection intensity value, which decreased with the distance, is approaching a constant value regardless of the distance. This can also be visually confirmed from the point cloud before and after correction shown in Figure 3(a) and (b). From the histogram of reflection intensity before and after correction shown in Figure 2(c), the reflection intensity value after correction approximately follows a normal distribution. This is thought to be because the reflection intensity values of points

(a) Point cloud imaging

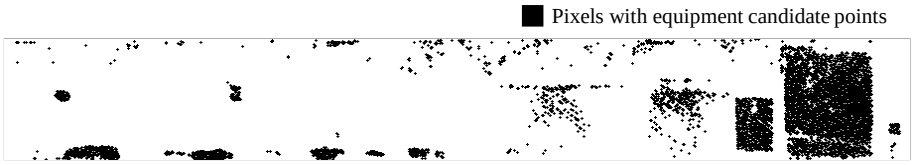

(b) Opening processing

(c) Closing processing

Figure 4. Morphological process

corresponding to areas with a large surface area and made of the same material were appropriately corrected.

3.4 Extraction of Equipment Candidate Points

From the normalized and corrected reflection intensity, it is considered that points corresponding to walls and ceilings are within a certain range from the average value, and points corresponding to building equipment are outside the range. Therefore, using the average value μ and standard deviation σ of the reflection intensity values, the points corresponding to equipment candidates are extracted by thresholding process. The threshold is set as $th=\mu\pm\alpha\sigma$, where α is a user-set parameter. Figure 3(c) shows an example of the extracted equipment candidate point cloud.

3.5 Imaging of Point Cloud

From the equipment candidate point cloud obtained in the process in the previous section, the point cloud is grouped by equipment. First, the candidate point cloud is projected onto the planes corresponding to wall or ceilings. And then the projection plane is gridded to create a binary image. The grid size (image resolution) was set to 2 cm. An example is shown in Figure 4(a). In the binary image, pixels that contain one or more points are shown in black, and the others are in white.

3.6 Extraction of Equipment Candidates

Table 1. Specification of scanners

Instrument	OS0 (Ouster)	VLP-16 (Velodyne)
Weight	430g	830g
Maximum distance	75m (80% reflectivity) 35m (10% reflectivity)	100m
Accuracy	±2.5cm (Lambert Target) ±5.0cm (Retroreflective Target)	±3cm
Field of view	360°×90°	360°×30°
Data acquisition rate	5.2M points/second	0.3M points/second

From the image obtained through the processing in the previous section, it can be seen that pixels other than the original equipment have been incorrectly extracted, and that there are areas where pixels identified as a single equipment have been disconnected. Therefore, morphological process is performed on the created binary image. Morphological process is based on dilation process which expands the binarized area by one pixel, and erosion process which shrinks inversely. In the opening process, it first iterates shrinking n times and then iterates the same number of expanding. This enables to remove isolated pixels. However, if the number of iterations is too large, even one piece of equipment may be divided into multiple pieces, or small equipment may be removed and cannot be extracted. On the other hand, in the closing process, it first iterates expanding and then shrinking n times. It has the effect of closing small holes in binary images and connecting unconnected components. However, if the number of repetitions is too large, adjacent multiple equipment will be connected and extracted as one. We set the number of iterations n to one to four depending on the dataset. Figure 4(b) and (c) shows images after opening and closing process respectively. It can be confirmed that the opening process removes isolated pixels and the closing process connects disconnected pixels.

Finally, the labeling process is used to assign a label to each connected component in the binary image and extract the equipment in the image. The same label is also assigned to the points inside the cells.

4 Results

4.1 Test Site and Scanners

The proposed method was applied to point cloud datasets obtained from two different scanners, Ouster OS0 and Velodyne VLP-16. Table 1 shows the specifications of each scanner.

OS0 has a viewing angle of 360° horizontally and 90° vertically and is prone to blind spots in the vertical direction. Therefore, as shown in Figure 5(a), the scanner mounted on a monopod was held at an angle so that the laser hit the ceiling surface vertically and scanned the underground parking lot while walking at a normal speed. As shown in Figure 5(b), the scanning point cloud of the wall surface of the underground parking lot (Data_A) used in the experiment was scanned by walking parallel to one direction while keeping a position about 6 m away from the target wall surface. The scan time was about 3 minutes, and the total number of points was about 1M points which was then reduced to 0.5M points after the sampling process. The smallest building equipment identified from this dataset was a rectangular fire extinguisher sign approximately 25 cm × 20 cm.

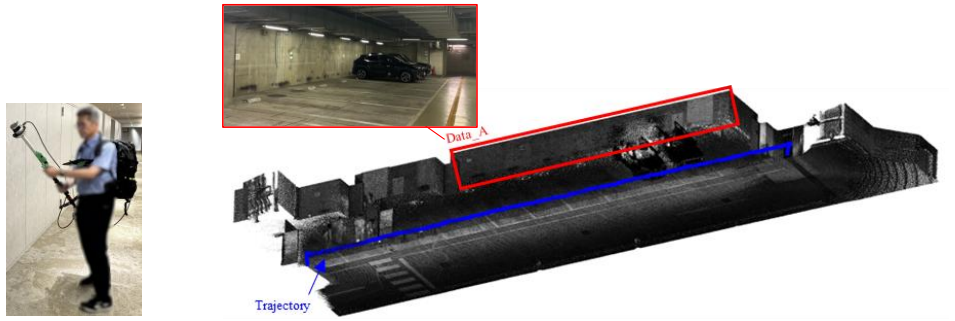

(a) scanning (b) Obtained point cloud and trajectory

Figure 5. Scanning with Ouster LiDAR OS0

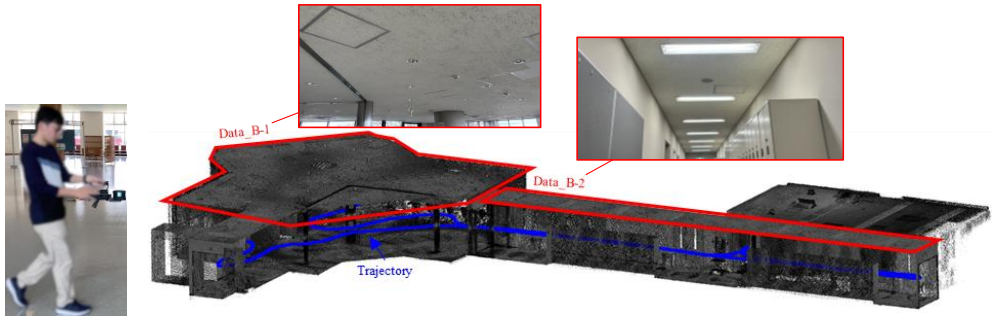

(a) scanning (b) Obtained point cloud and trajectory

Figure 6. Scanning with Velodyne LiDAR VLP-16

On the other hand, VLP-16 has a viewing angle of 360° horizontally and 30° vertically, and this also tends to have blind spots in the vertical direction. Therefore, as shown in Figure 6(a), a mobile laser scanner Hovermap from Emesent equipped with the VLP-16 was held parallel to the floor and scanned the interior of the university building while walking at a normal speed. By rotating the VLP-16 attached to the tip of the Hovermap, it is possible to evenly irradiate a laser over a 360° × 360° area. Figure 6(b) shows the scanning point cloud of the ceiling surface of the elevator hall (Data_B-1) and the ceiling surface of the corridor (Data_B-2) used in the experiment. The scanning time was about 5 minutes. The total number of points in Data B-1 was about 4M and then sampled to 1.3M. The total number of points in Data B-2 was about 2M and sampled to 0.6M. The smallest building equipment identified from this dataset was a circular fire alarm with a diameter of approximately 10 cm.

4.2 Results of Intensity Correction

Figure 7 shows the results of comparing the reflection intensity distribution of point clouds scanned using OS0 and VLP-16. A study by Viswanath et al. (Viswanath et al., 2024) shows that there are significant differences in the reflection intensity values obtained from these two scanners. The reflection intensity values obtained with Ouster LiDAR are raw data that have not been pre-calibrated, while those obtained with Velodyne LiDAR are data that have been calibrated for distance and laser power, as described in the manual. The data obtained from OS0 showed a trend like that

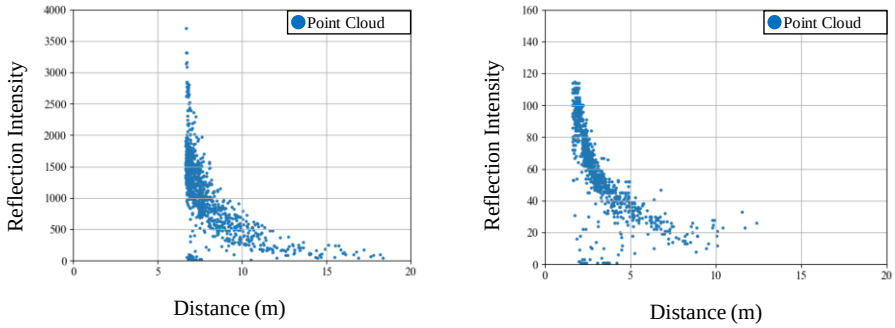

(a) Ouster LiDAR (b) Velodyne LiDAR

Figure 7. Reflection intensity distribution of Ouster and Velodyne LiDAR

Table 2. Results of reflection intensity correction

Instrument	Target area		Average	Standard deviation
Ouster LiDAR	Wall of underground parking (Data_A)	Before	1101.0	605.5
		After	904.9	309.3
Velodyne LiDAR	Ceiling of elevator hall (Data_B-1)	Before	66.4	27.2
		After	61.9	16.6
	Ceiling of the hallway (Data_B-2)	Before	78.7	22.5
		After	76.0	16.6

described in the paper, as shown in Figure 7(a). However, the data obtained from VLP-16 showed a tendency for the reflection intensity to decrease as the distance increases as shown in Figure 7(b). Therefore, as introduced in Section 3.3, the reflection intensity was corrected using the method of Wan et al. (Wan et al., 2019) for both data sets.

Table 2 shows the results of reflection intensity correction. Data_A was corrected using the 6th-order equation since we found it tightly approximated the sampled points from experiments than 3rd-order. Comparing the initial and corrected reflection intensity, the standard deviation is smaller after correction for both Ouster and Velodyne LiDAR, confirming the correction effect. Therefore, it was found that simultaneous correction of distance and incident angle using Equation (5) can be applied when scanning while keeping the distance between the scanning device and the surface constant. As in Figure 2(c), it was also confirmed visually that the corrected reflection intensity roughly follows a normal distribution.

4.3 Results of Equipment Detection

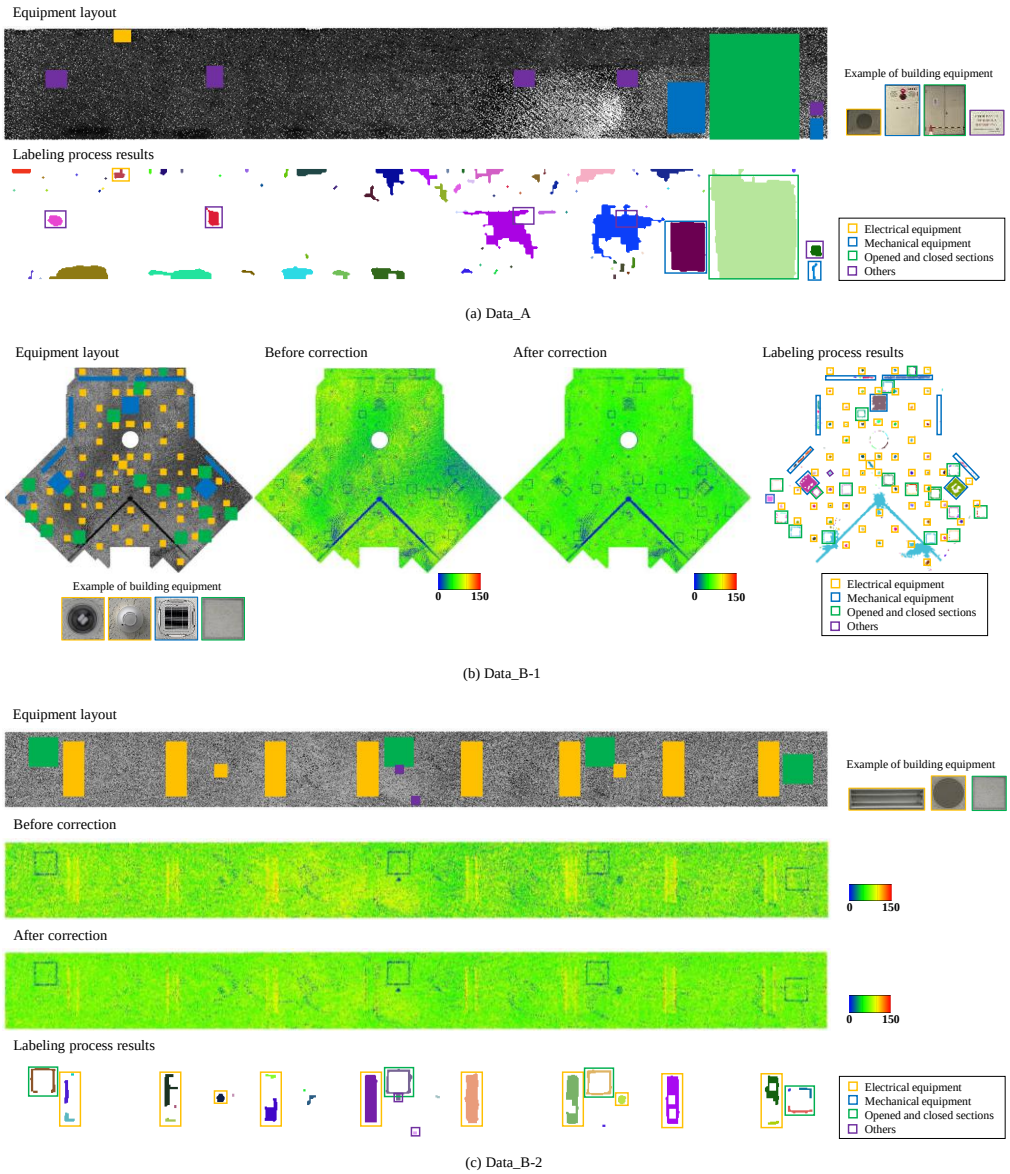

Figure 8. Visual evaluation of building equipment

Figure 8 shows the results of visual detection of building equipment. The equipment layout was visually compared with the actual site images. And if more than one labeled pixel exists in the corresponding position, the building equipment was considered to have been detected correctly. Table 3 shows the detection results for building equipment. We set α=1.0 for Data_A and α=2.0 for Data_B-1 and Data_B-2.

Overall, many regions were extracted compared to the actual number of equipment. The correct detection rates were large in Data_B-1 and Data_B-2, which may be since the region was divided into multiple parts and extracted for one equipment. Conversely, there were on miss-detections. Over detections differed greatly depending on the data.

Table 3. Result of building equipment detection

	Data_A		Data_B-1		Data_B-2	
Number of equipment	9	-	87	-	16	-
Number of extracted regions	77	855.6%	172	197.7%	28	175.0%
Correct detection	9	100.0%	124	142.5%	23	143.8%
Miss detection	0	0.0%	0	0.0%	0	0.0%
Over detection	70	90.9%	48	27.9%	5	17.9%

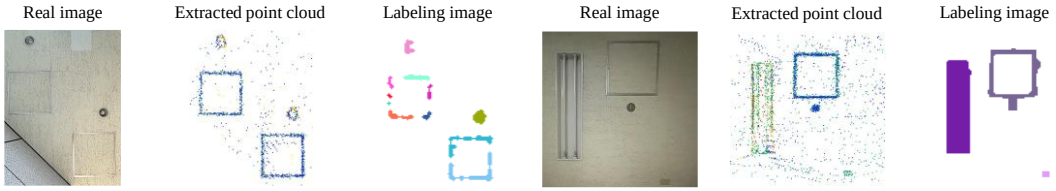

(a) Example of split label (b) Example of combined label

Figure 9. Results of labeling process

As for Data_A, our method could detect nine all equipment. However, two of them could not detect only equipment correctly and extracted as wide areas including its surrounding wall surface. The reason is that cars were parked in front of the signs while scanning. And it made it difficult to scan correctly because they were obstructed, and the reflection intensity value of the corresponding wall area was abnormally low. Over detection rates were 90.9%. This is because the material of the wall surface used in this study is concrete which is easily stained. And it is thought that intensity value varies depending on the degree of stain and some portions of the stained area were detected as equipment candidates. Our method assumes that the target area is composed of the same material, but this concrete surface does not follow it due to the stains. Therefore, it is difficult to extract only the equipment by extracting only the reflection intensity.

As for Data_B-1 and Data_B-2, it has low over detection rates of 27.9% and 17.9% respectively. Since these indoor data well follow the assumption, good results were obtained. The number of detected regions is large compared to that of equipment, and correct detection rates were also large, i.e., 197.7% and 175.0% respectively. This is due to the image processing aspects of the proposed method rather than the intensity correction. Even if morphological process is applied, the pixels are not sufficiently connected, and the labels are detected as divided for an equipment. For example, this was typically seen in cases of ceiling inspection hatches which is composed of long and thin metal frames, as shown in Figure 9(a). Conversely, the multiple pieces of equipment were sometimes labeled as a single unit when they were located close to each other, as shown in Figure 9(b). Another example is shown in Figure 8(b). In this figure, our method did not work well for the pillars of the fire shutters made of metal and detected a wide area including the surrounding equipment as a single unit. Therefore, it is necessary to revise the concatenation conditions of the pixels extracted as equipment candidates for more correct detection.

5 Conclusions

In this study, we proposed a method of detecting building equipment based on reflection intensity correction with the aim of constructing detailed BIM from MLS scanned point cloud. In the proposed

method, we first demonstrated that the effects of scanning distance and incident angle contained in the laser reflection intensity can be eliminated from the measurement point cloud of ceilings and walls obtained by MLS using polynomial approximation. And we verified that the reflection intensity of flat ceilings and walls made of the same material can be corrected to approach a constant value. We also demonstrated that the corrected reflection intensity can be used to detect building equipment without omission through thresholding and morphological process. An advantage of the proposed method is that it uses MLS, so it can measure a wide area more efficiently than conventional methods using TLS or SfM. In addition, compared to conventional methods using images and deep learning, it has the advantage that no preparation of training data is required and extraction process can be performed without being affected by lighting or shadows.

A limitation of the proposed method is the case where there is variation in the reflection intensity of the background as shown in the example of Figure 8. When there are differences in the color or material in the background, such as stains on the wall or deteriorated paint, and the reflection intensity of the background varies, it may erroneously extract things other than the equipment. A possible solution to this problem is to use the image and reflection intensity in combination for comprehensive analysis, rather than using them alone. Future issues include removing regions where equipment is over-detected and dealing with regions where equipment is divided into multiple parts. We will also compare the method with other correction methods and consider its application to buildings with non-flat shapes. We also need to consider how to classify the obtained facility classes.

Acknowledgments

The authors would like to express their gratitude to KYUDENKO CORPORATION for their support in carrying out this study.

References

Akiyama, R., Date, H., Kanai, S., and Yasutake, K. (2023). FOOTPRINT DETECTION OF CEILING EQUIPMENT FROM TLS POINT CLOUDS, *Proceedings of the 5th International Conference on Civil and Building Engineering Informatics*, 465-470.

Anjanappa, G., Nikoohemat, S., Oude Elberink, S., Voûte, R. L., and Lehtola, V.V. (2023). NEEDLE IN A HAYSTACK: FEASIBILITY OF IDENTIFYING SMALL SAFETY ASSETS ROM POINT CLOUDS USING DEEP LEARNING, *ISPRS Annals of the Photogrammetry, Remote Sensing and Spatial Information Sciences*, X-1/W1-2023, 461-468.

Bai, J., Niu, Z., Gao, S., Bi, K., Wang, J., Huang, Y., and Sun, G. (2023). An exploration, analysis, and correction of the distance effect on terrestrial hyperspectral LiDAR data, *ISPRS Journal of Photogrammetry and Remote Sensing*, 198, 60-83.

Di Stefano, F., Chiappini, S., Gorreja, A., Balestra, M., and Pierdicca, R. (2021). Mobile 3D scan LiDAR: a literature review, *Geomatics, Natural Hazards and Risk*, 12 (1), 2387–2429.

Hossain., M., Ma., T., Watson., T., Simmers., B., Khan., J. A., Jacobs., E. and Wang., L. (2021). Building Indoor Point Cloud Datasets with Object Annotation for Public Safety, *Proceedings of the 10th International Conference on Smart Cities and Green ICT Systems (SMARTGREENS 2021)*, 45–56.

Jeong, J., and Kim, A. (2018). LiDAR Intensity Calibration for Road Marking Extraction, *2018 15th International Conference on Ubiquitous Robots (UR)*.

Pan, Y., Braun, A., Brilakis, I., and Borrmann, A. (2022). Enriching geometric digital twins of buildings with small objects by fusing laser scanning and AI-based image recognition, *Automation in Construction*, 140, 104375.

Tan, K., and Cheng, X. (2015). Intensity data correction based on incidence angle and distance for terrestrial laser scanner, *Journal of Applied Remote Sensing*, 9, 094094.

Tan, K., and Cheng, X. (2020). Distance Effect Correction on TLS Intensity Data Using Naturally Homogeneous Targets, *IEEE GEOSCIENCE AND REMOTE SENSING LETTERS*, 17 (3), 499-503.

Viswanath, K., Jiang, P., PB, S., and Saripalli, S. (2024). Off-Road LiDAR Intensity Based Semantic Segmentation, arXiv:2401.01439 [cs.CV].

Wan, R., Huang, Y., Xie, R., and Ma, P. (2019). Combined Lane Mapping Using a Mobile Mapping System, *Remote Sens. 2019*, 11(3), 305.